Mechanic Waves in Sand, 3d Simulations

O Mouraille[a,*], W A Mulder[b] & S Luding[a]

[a] Particle Technology, Nanostructured Materials, DelftChemTech, TUDelft, Julianalaan 136, 2628 BL Delft, Netherlands

[b] Applied Geophysics and Petrophysics, Civil Engineering and Geotechnology, Delft, Netherlands

E-mail: * o.mouraille@tnw.tudelft.nl

Abstract. The sound propagation mechanisms inside dense granular matter are challenging the attempts to describe it because of the discrete nature of the material. Phenomenona like dissipation, scattering, and dispersion are hard to predict based on the material state and/or properties and vice-versa. We propose here a simulation method using dynamic discrete elements in order to get more insight in this problem. The idea is to examine a small perturbation created on one side of a dense, static packing of grains, during its propagation and when it arrives at the opposite side. A pertinent choice for the boundary conditions allows us to apply longitudinal or shear perturbations in order to select the respective modes of information propagation. Moreover the rotational degree of freedom permits to observe the role of rotations in the wave propagation. The propagation of rotational energy in itself is studied as well. The control on the inter-particle forces like contact potential, cohesion and friction make it possible to observe the effect of these micro-parameters on the macro-behavior at the wave scale. Simulations performed on different types of packings - regular and random poly-disperse - already show the consequences of anisotropy and allow its characterization. The goal of this study is a better understanding of the numerous sound propagation mechanisms in granular materials.

1. Introduction

Sand, like other granular materials consists of many individual grains that interact with each other via contact forces. A continuum description [2] of such discrete granular materials is generally needed in field application because of the size of the system considered and the prohibitively large number of particles involved. Hence starting from a simulation at the micro level, where only a small subsystem is considered – a representative elementary volume (REV) – the goal is a "micro-macro" transition for the applications, which contains micro-informations also in the framework of the macroscopic picture. This holds in particular for information propagation in granular materials. The work presented here involves a regular structured packing on which wave phenomenona are tested. In the following, section 2 describes the discrete MD (Molecular Dynamics) model used and the granular packing Section 3 details the difference between modes of agitation and propagation (compressive/shear). The dispersion relation is extracted from the data and compared to theoretical predictions.

2. The simulation tool

2.1. The DEM Model

The simulation tool used here is a Molecular Dynamic code using a linear normal contact law including a linear spring and a linear dashpot: $f_i^n = k\delta + \gamma_0\dot{\delta}$, with spring constant k and some damping coefficient γ_0. The half-period of a vibration around the equilibrium position leads to a typical response time $t_c = \pi/\omega$, with $\omega = \sqrt{(k/m_{ij}) - \eta_0^2}$ the eigenfrequency of the contact, the reduced mass $m_{ij} = m_i m_j/(m_i + m_j)$, and the rescaled damping coefficient $\eta_0 = \gamma_0/(2m_{ij})$. The energy dissipation during a collision, as caused by the dashpot, leads to a restitution coefficient $r = -v_n'/v_n = \exp(-\eta_0 t_c)$, where the prime denotes the normal velocity after a collision. In order to take into account the rotation of particles, forces in the tangential direction are considered. They can be implemented in the spirit of Ref. [3], where a tangential spring was introduced to account for static friction. For related literature, see Refs. [4, 5, 6].

2.2. System configuration

The system considered here is a dense, static packing of grains contained in a cuboid. The structure chosen here has a body centred cuboid lattice structure: square-layers in the x-y-plane are stacked on top of each other (in z-direction), such that each layer fits into the holes of the one below, and each second layer is just a z-shifted copy of the original. The distance between square layers is $l_0 = d/\sqrt{2}$ for a particle diameter d. Based on a particle-centred square in the first layer, a unit-cell (cuboid) therefore has a volume $V_u = \sqrt{2}d^3$ and contains 2 particles with volume $2V_p = (\pi/3)d^3$ such that the volume fraction is $\nu = 2V_p/V_u = \pi/(3\sqrt{2}) \approx 0.74$.

This structure will not change in the simulations described below, since the case of

small amplitude perturbations is considered. Even though all contacts have the same predefined overlap, the packing is self-similar in the x- and y-directions, but not in the z-direction, hence it is an anisotropic system (see Fig. 1).

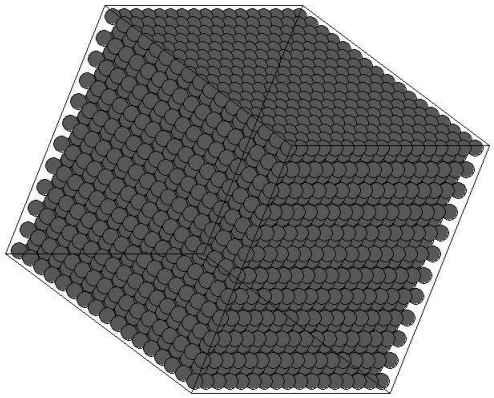

Figure 1. Snapshot of a typical body centred cuboid packing.

Before a small amplitude sound wave is agitated, the system must be relaxed first to a reasonable static equilibrium state, for example with a desired isotropic confining stress $\sigma^0_{xx} = \sigma^0_{yy} = \sigma^0_{zz} = P_0$, such that the contact overlaps are still much smaller than the particle diameter, $\delta/d \approx 10^{-3}$. Periodic boundary conditions are used and so the stress is perfectly isotropic. 3.4).

Waves are agitated by applying a small perturbation at one side of the system, i.e., by shifting a layer of particles. The wave vector and the wave propagation direction are perpendicular to the agitated layer. Compressive (P) and shear (S) modes can be triggered by directing the perturbation either parallel or perpendicular to the wave propagation direction. Fig. 1 shows a regular packing in the x, y-planes ($l_x = l_y = 17d$ and $16d$) and 23 layers in z-direction ($l_z = 23l_0$). However the typical packing used is much longer in the z-direction which allows to study the wave for a longer time and larger distances. We checked that the results do not depend on the extension in x- and y-direction by comparing simulations with different size l_x, l_y. Therefore $l_x = l_y = 5d$ was used in order to reduce the number of particles. Such a long but thin system contains only $N = 3200$ particles with radius $a = d/2 = 0.001$m. The mass of a spherical particle is $m = \rho_0(4/3)\pi a^3$, with the material density $\rho_0 = 2\,10^3$ kgm^{-3}. The total mass of the system is thus $M \approx 0.027\,$kg. The stiffness material parameters in normal and tangential direction are $k = 10^5\,\mathrm{N\,m^{-1}}$ and $k_t = 0.2k$ (tangential spring stiffness, if activated). Dissipation $\gamma_t = \gamma_0 = 0$ is used if not explicitly specified. This leads to a typical (two-particle) contact duration $t_c = 2.033\ 10^{-5}$ s and collision frequency $\omega_c = 150\,$kHz. (The oscillation frequency of a particle in a crystal, with more than one contact, is higher.) For reliable numerical results, the criterion for the integration time-step is $\delta t_{\mathrm{MD}} < \frac{t_c}{50} \approx 4.10^{-7}$ s. Since the wave propagation simulations are relatively fast, $\delta t_{\mathrm{MD}} = 10^{-8}\,$s is used, not so much for an improved accuracy but to allow for a

very high data-output frequency if desired.

3. RESULTS

In this section, a typical wave propagation simulation is presented. The effect of dissipation and friction are briefly discussed and the wave propagation speed is determined. Furthermore, the space- and time-Fourier transforms of the wave are presented and interpreted.

3.1. Wave propagation simulation

The strain-controlled perturbation of the layer, creates a plane compressive stress pulse (P wave) which propagates in the system in z direction, see Fig. 2. More specific, a x, y-layer is shifted by $\Delta z/d = 10^{-4}$. This displacement amplitude, Δz, that agitates the wave is still small as compared to the typical overlap $\Delta z/\delta = 10^{-1}$. stress, displacement, kinetic energy, etc. Fig. 2 shows the scaled normal stress versus time at different positions along the wave propagation direction.

As consequence of the use of periodic boundaries, two opposite ends of the system are connected, and a tensile wave would travel in the direction opposite to the compressive pulse. In order to avoid this, and to maximise the distance that can be traveled by a pulse, two layers of particles at the opposite ends of the system are fixed – the other two directions remain periodic. This avoids the tensile pulse, but not boundary reflections that lead to an oscillating "coda" traveling after the primary pulse, see Fig. 2.

change, The analysis presented in the following considers only the initial, undisturbed wave propagation, since interference with the reflected wave would disturb the signal. The shape of the signals and the wave speed will be examined next.

3.2. Analysis of time signals

The pulse in Fig. 2 consists of two parts. The first strong peak corresponds to the increase of stress when the wave front arrives at the recording position. The second part, the "coda" of the signal, consist of secondary wave fronts created by the oscillation of the layer closest to the shifted layer (that stays fixed after the shift). Its intensity decays with time. During propagation, the first peak-amplitude decreases and its width increases. Note that there is no active dissipation, so that the described signal behaviour is caused by the frequency-dependent nature of the wave (dispersion), and the particular boundary condition. One way to define the wave speed is to measure the time it takes the peak of the first pulse to travel a certain distance. Plotting the z-position of each peak against the time t when it reaches that position (not shown here) gives an almost straight line. The slope of this line then gives the speed V_p during propagation, see Fig. 3. Just assuming a constant speed (a linear fit to the z, t-data) leads to $V_{p1} \approx 216\,\mathrm{m/s}$. This disregards the interesting acceleration of the pulse early during propagation. In Fig. 3,

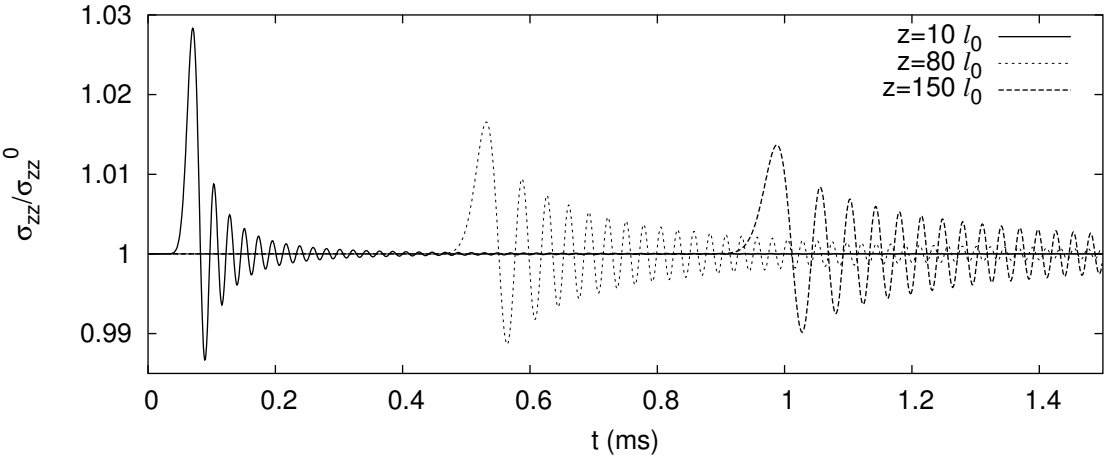

Figure 2. Normal stress (σ_{zz}) scaled by the equilibrium stress (σ^0_{zz}) as function of time at different positions $z/l_0 = 10$, 80, and 150, with the distance from the sender, z, and the layer distance l_0.

the wave speed is compared to the simply fitted V_{p1} and to the theoretical prediction V_{pz} as obtained from a micro-macro transition [8].

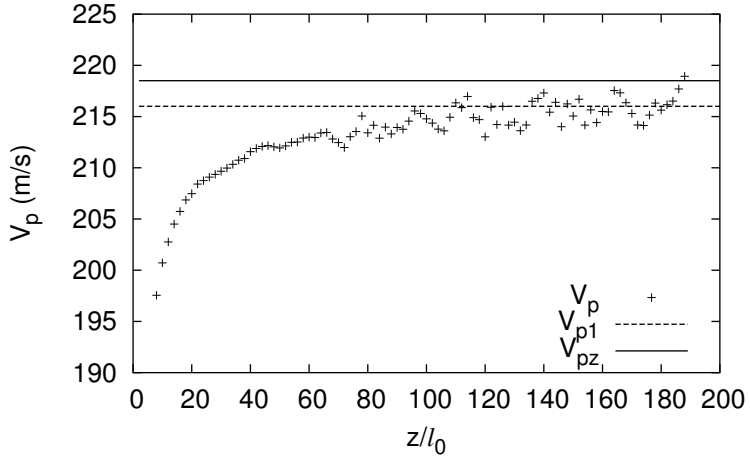

Figure 3. From the simulation see Fig. 2, the speed of the first peak maximum, V_p, is plotted as a function of the distance from the source. (A center-weighted average over five layers is used here. Also a higher output frequency was needed to obtain reliable data). The dashed line indicates the average speed, V_{p1}, and the solid line is the theoretical prediction, V_{pz}.

3.3. Fourier space

In order to study the frequency dependence of the P wave in our system, we performed a Fourier analysis in time and space. ¿From a t, x data set in a system of length $l_z = 200\, l_0$, with spacing $\Delta z = l_0 = d/\sqrt{2}$, every layer position is taken into account, i.e., 200 points

in x-space are available. The time-window $0 \leq t \leq t_{max}$, with time step $\Delta t = 10^{-6}$ s and $t_{max} = 1199\Delta t$ is chosen, i.e., 1200 data points, such that the wave has not yet arrived at the end of the system: reflections are not included in the signal.

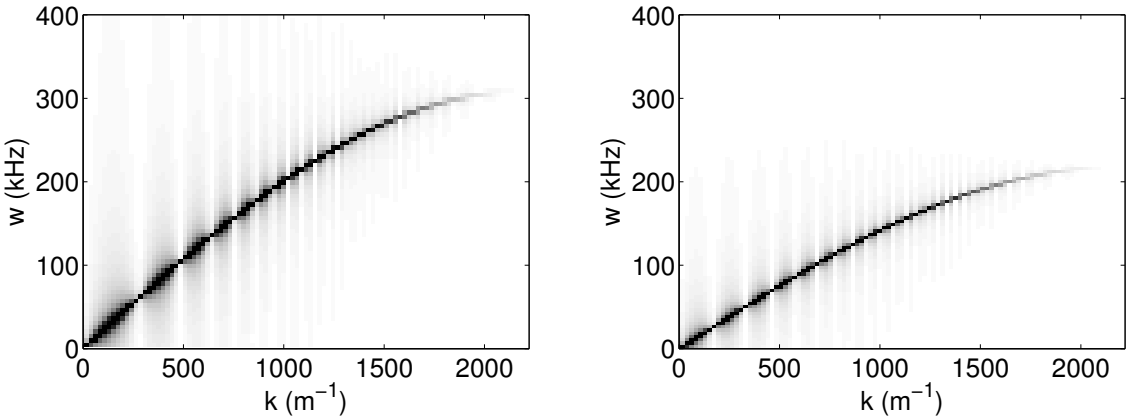

Figure 4. Dispersion relations (grey-scale corresponds to the amplitude of the Fourier coefficients) for P wave (Left) and S wave (Right) in an anisotropic packing, propagating in z direction.

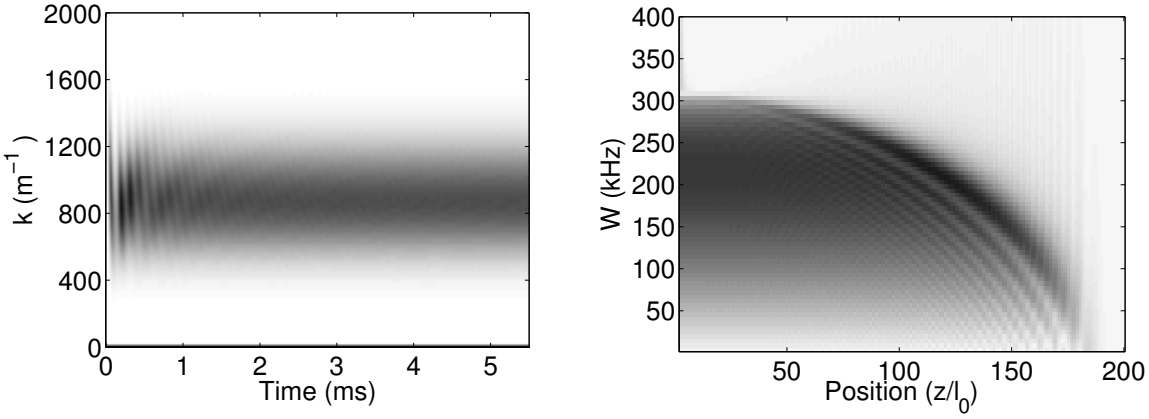

Figure 5. Wave number versus time (left) and Frequency versus position (right), for the P-wave from Fig. 4 (grey-scale corresponds to the amplitude of the Fourier coefficients).

The dispersion relations are obtained for P and S waves propagating in z direction, see Fig. 4 (Left) and (Right), respectively. The MATLAB function `fft2` can be used, which returns the Fourier coefficients in an indexed ω, k-field $F(\omega, k)$ of the same size as the input t, x data. Transformation to frequency and wave-number is performed by multiplying the index with $\Delta\omega = 2\pi/t_{max}$ and $\Delta k = 2\pi/l_z$. Special attention has to be taken that the $\omega = 0$ and $k = 0$ indices are properly shifted to zero.

In order to obtain the sine fit to the Fourier data, the locations of the maximal Fourier coefficients on the frequency axis were determined by a power-law weighted

average in Ref. [8]. The maximal frequencies are $\omega_0^{pz} = 309132\,\mathrm{s}^{-1}$ and $\omega_0^{sz} = 218437\,\mathrm{s}^{-1}$, and the minimal wavelength is $2l_0$. The quality of the fit is impressive with respect to both shape and magnitude of ω_0. The sine function is consistent with the theoretical work by Suiker et al. [1], where the dispersion relation for 2D lattices is discussed.

The acceleration of the wave observed can be related to an increasing wave-length during propagation. With other words, using the dispersion relation, a typical wave-number can be related to a local wave propagation speed. The waves are agitated with a minimal wave-length and rapidly adapts to a speed of $V_{pz}^{\omega}(k) \approx 208\,\mathrm{m/s}$ at $z/l_0 \approx 15$, and accelerates further on, see Fig. 3. This picture becomes more clear when the wave-number is plotted against time in Fig. 5 (Left). There are strong oscillations visible at the beginning, but after about 2 ms, the wave has adapted to its preferred spectrum of wave-numbers (wave-lengths), with a maximum around 900 m^{-1}. More quantitatively, using the fitted dispersion relation leads to a corresponding wave number

$$k\left(\frac{z}{l_0} = 15\right) \approx \frac{2}{l_0} \arccos \frac{V_{pz}^{\omega}(k)}{V_{pz}^{\omega}(0)} \approx 885\,\mathrm{m}^{-1}\ ,$$

corresponding to a wavelength of $\lambda_{15} \approx 10 l_0$, consistent with the rough average obtained from the oscillation duration of the signal at $z/l_0 = 15$. The wave adapts to a shape with a preferred wave-number and a width in wave-numbers of around 100 - 150 m^{-1}.

The typical wavelength is increasing while the wave (slightly) accelerates. The fine-structure in the wave-number against time plot was not visible in the dispersion relation, which shows that the frequency dependency of sound waves in a (regular-lattice) particulate material is such that low-frequency/long wavelength components are faster than the high-frequency wave components with smaller wavelength. With other words, narrow pulses will not travel fast, and high frequency perturbations ($\omega > \omega_0$) will practically not propagate at all. This last statement is also evident when plotting frequency against position in Fig.5 (Right). The high frequency components could not travel that far as the low frequency ones. Again, a rich fine-structure is visible in the plot – mostly at the wave-front.

This detailed quantitative study of the classical dispersion relation in the special situation of a crystal is only the basis for future research on sound propagation in polydisperse, disordered, frictional and anisotropic granular media.

4. CONCLUSION

Wave propagation was examined in three dimensional regular (crystal) monodisperse packings of spheres, for compressive (P) and also shear (S) propagation modes. For both P- and S-wave speeds, quantitative agreement was obtained between simulations and theoretical predictions based on a micro-macro computation of the stiffness material tensor for the anisotropic lattice. Also the dispersion relation agrees perfectly well with theory and the observed acceleration of the travelling wave can be related to the dispersion and widening of the pulse: the initial spectrum with short wave-lengths

adapts to a wider pulse that travels somewhat faster. The fine-structure in the k-spectrum for short times and in the ω-spectrum at the wave front still has to be understood, as well as the adaptability of the present method to more realistic systems.

ACKNOWLEDGEMENTS

Helpful discussions with G. Herman and A. Suiker are appreciated. This work is part of the research programme of the Stichting voor Fundamenteel Onderzoek der Materie (FOM), financially supported by the Nederlandse Organisatie voor Wetenschappelijk Onderzoek (NWO) and the Stichting Shell Research.

References

[1] A. S. J. Suiker, A. V. Metrikine, and R. de Borst. Comparions of wave propagation characterisitcs of the Cosserat continuum model and corresponding discrete lattice models. *Int. J. of Solids and Structures*, 38:1563–1583, 2001.

[2] A. L. Fetter and J. D. Walecka. *Theoretical Mechanics of Particles and Continua*. Dover Publisher, 2003.

[3] P. A. Cundall and O. D. L. Strack. A discrete numerical model for granular assemblies. *Géotechnique*, 29(1):47–65, 1979.

[4] L. Brendel and S. Dippel. Lasting contacts in molecular dynamics simulations. In H. J. Herrmann, J.-P. Hovi, and S. Luding, editors, *Physics of Dry Granular Media*, page 313, Dordrecht, 1998. Kluwer Academic Publishers.

[5] S. Luding. Micro-macro transition for anisotropic, frictional granular packings. *Int. J. Sol. Struct.*, 41:5821–5836, 2004.

[6] S. Luding. Anisotropy in cohesive, frictional granular media. *J. Phys. Condensed Matter*, 17(24):S2623–S2640, 2005.

[7] O. Mouraille and S. Luding. Dispersion relations for frictional, random granular media. in preparation.

[8] O. Mouraille and S. Luding. Sound wave acceleration in granular materials. submitted to JSTAT, 2006.

[9] P. A. Vermeer, S. Diebels, W. Ehlers, H. J. Herrmann, S. Luding, and E. Ramm, editors. *Continuous and Discontinuous Modelling of Cohesive Frictional Materials*, Berlin, 2001. Springer. Lecture Notes in Physics 568.

[10] S. Luding. Granular media: Information propagation. *Nature*, 435:159–160, 2005.

[11] O. Mouraille and S. Luding. Sound propagation in dense, frictional granular materials. In R. Garcia-Rojo, H. J. Herrmann, and S. McNamara, editors, *Powders and Grains 2005*, page 319, Leiden, 2005. A. A. Balkema Publishers.